

Influence of partial fluorination on growth modes of organic molecules on amorphous silicon dioxide

Mila Miletic 


Research Group Simulations of Energy Materials, Helmholtz-Zentrum Berlin für Materialien und Energie,
Hahn-Meitner-Platz 1, D-14109 Berlin, Germany
and Institut für Physik, Humboldt-Universität zu Berlin, Newtonstrasse 15, 12489 Berlin, Germany

Karol Palczynski 

Research Group Simulations of Energy Materials, Helmholtz-Zentrum Berlin für Materialien und Energie,
Hahn-Meitner-Platz 1, D-14109 Berlin, Germany

Joachim Dzubiella[†]

Applied Theoretical Physics - Computational Physics, Albert-Ludwigs-Universität Freiburg,
Hermann-Herder Straße 3, D-79104 Freiburg, Germany
and Research Group Simulations of Energy Materials, Helmholtz-Zentrum Berlin für Materialien und Energie,
Hahn-Meitner-Platz 1, D-14109 Berlin, Germany

 (Received 21 October 2021; revised 9 March 2022; accepted 9 March 2022; published 24 March 2022)

We study the influence of fluorination on nucleation and growth of the organic parasexiphenyl molecule (*p*-6P) on amorphous silicon dioxide (*a*-SiO₂) by means of atomistically resolved classical molecular dynamics computer simulations. We use a simulation model that mimics the experimental deposition from the vapor and subsequent self-assembly onto the underlying surface. Our model reproduces the experimentally observed orientational changes from lying to upright standing configurations of the grown layers. We demonstrate that the increase in the number of fluorinated groups inside the *p*-6P leads to a smoother, layer-by-layer growth on the *a*-SiO₂ surface: We observe that in the first layers, due to strong molecule-substrate interactions the molecules first grow in chiral (fan-like) structures, where each consecutive molecule has a higher angle, supported by molecules lying underneath. Subsequently deposited molecules bind to the already standing molecules of the chiral structures until all molecules are standing. The growth of chiral islands is the main mechanism for growth of the fluorinated *p*-6P derivative, while the *p*-6P, due to the lower interaction with the underlying substrate, forms less chiral structures. The higher degree of chirality leads to a lower-energy barrier for step-edge crossing for the fluorinated molecules. We find that partial fluorination of the *p*-6P molecule can, in this way, significantly alter its growth behavior by modifying rough, three-dimensional growth into smooth, layer-by-layer growth. This has implications for the rational design of molecules and their functionalized forms, which could be tailored for a desired growth behavior and structure formation.

DOI: [10.1103/PhysRevMaterials.6.033403](https://doi.org/10.1103/PhysRevMaterials.6.033403)

I. INTRODUCTION

Hybrid structures of organic and inorganic semiconductors (HIOS) have shown enormous application potential in recent years [1–3]. Combining the favorable properties of individual materials into a single conjugate makes it possible to realize device properties that cannot be achieved with either material class alone. To control the properties and functions of HIOS, it is necessary to know the molecular structure and to understand the molecule-molecule interactions and the molecule-surface interactions at the hybrid interface during the interface formation. Then controlling the properties and functions of HIOS can be accomplished by a combination of chemical functionalization of the organic adsorbates and a careful selection of the underlying surface.

For instance, the hydrogens in the *meta* positions of both terminal phenyl groups of the prototypical organic parasexiphenyl (*p*-6P) molecule can be substituted by fluorine atoms to introduce two local dipole moments at both terminal groups [4,5]. This, in turn, changes the degree of diffusion-anisotropy of the molecule on the inorganic zinc oxide (10 $\bar{1}$ 0) surface, which leads to differences in the growth morphology [6]. Films of *p*-6P are characterized by a three-dimensional (3D) morphology with mound-like crystalline islands and a rather rough surface. In contrast, the fluorinated derivative (*p*-6P4F) grows in a layer-by-layer mode with a smooth, two-dimensional (2D) morphology [7]. Various other fluorinated derivatives of *p*-6P show a strong impact of the fluorine positions on the structures of the thin films and on their energetics [8]. Strong molecule-surface interactions can lead to further interesting growth phenomena: surface-induced polymorphs [7,9–16], wetting layers, i.e., flat-lying molecules at the interfaces [17,18], or the formation of defective islands with tilted or disordered edges [19].

*karol.palczynski@helmholtz-berlin.de

†joachim.dzubiella@physik.uni-freiburg.de

Next to the important influence of the underlying surface, the grown morphologies also depend critically on the fabrication conditions including deposition rates, substrate temperature, chamber pressure, and thermal treatments [20–26]. For instance, recent studies reported that, by lowering the substrate temperature, adsorbed molecules can be controlled to adopt a lying orientation on an amorphous silicon dioxide (a -SiO₂) surface rather than a standing orientation [27,28]. Nagai *et al.* [29] also demonstrated that the ratio of standing molecules to lying molecules increases with increasing temperature, as observed in grown films of pentacene on a -SiO₂ studied by p -polarized multiple-angle incidence resolution spectrometry. This suggests that the nucleation of standing-oriented islands is thermally activated at a constant deposition rate. Furthermore, at low-enough temperatures, mainly the lying orientation occurs and the final film structure consists of lying molecules. Nagai *et al.* further observed that the temperature dependence of the probability to nucleate in standing orientation has an Arrhenius behavior, from which a collective energy barrier for reorientation can be deduced. Interestingly, they observed increased migration of adsorbates to distant existing nuclei at higher temperatures enabled by the increased surface diffusion. Under diffusive conditions at sufficiently high temperatures, molecules can form larger, stable islands with optimal configurations which facilitates the orientational change. The temperature-dependent evolution of the island size can be explained by the diffusion-mediated growth model, as reported by Tejima *et al.* [30]. In this model, the nucleation density depends on the diffusivity of molecules and the deposition rate. When the deposition rate is constant, the island size increases with the growth temperature because island growth is promoted by high diffusivity.

Although there is an ample amount of experimental studies on growth of organic molecules with different structural and chemical properties, insights on the microscopic features and nanoscale dynamics of molecular growth and thin-film formation of HIOS are still rare. Classical molecular dynamics (MD) computer simulations can circumvent experimental limitations and provide a nanoscale picture of the processes involved in thin-film formation. The employed force fields must be good enough to reproduce spontaneously self-assembled room-temperature solid crystals on the inorganic surfaces, as observed in experiments. MD simulations further require an adequate sampling of the vast configurational space related to the formation of complex molecular structures. This is a challenge for the current simulation methods because of the computational cost necessary for this. Even then, the limited simulation time may not be sufficiently long to allow the strongly attractive molecules to arrange into ordered positions on the surface. Recent simulation studies indicate that relevant growth events can be successfully reproduced on timescales accessible in atomistic simulations, at least for pentacene and sexithiophene molecules [31,32]. The computation time required for this, however, lies in the order of 10² to 10³ hours. Muccioli *et al.* [31] demonstrated that, in pentacene deposition on a C₆₀ crystal surface, the molecules self-assemble into crystal nuclei, closely resembling the bulk crystal structure. The authors stressed that the observed deviations in the self-assembled crystal structures could originate from surface distortions or imbalances in the chosen force field.

Roscioni *et al.* [18] additionally showed that the vapor deposition of pentacene molecules onto the a -SiO₂ surface results in the correct room-temperature bulk crystal structure in the first two adsorbed layers, with unit-cell dimensions consistent with experimental measurements. Furthermore, Pizzirusso *et al.* [32] showed that sexithiophene molecules spontaneously arranged into an ordered crystal-like structure at room temperature, consistent with experimental densities and global molecular orientations. Simulations of sexithiophene on C₆₀ by D’Avino *et al.* [19] revealed the spontaneous formation of wetting layers and of chiral, propeller-like distorted, crystalline islands with tilted edges. When enough molecules were deposited, the chiral phases expanded into crystalline monolayers with well-defined and uniform molecular orientations.

Despite these efforts, important questions still remain. Why do certain chemical modifications, such as the fluorination of the p -6P, alter the growth modes and the structures of the thin films? What mechanisms lead to the change from a 3D growth morphology to a 2D morphology? What role do the molecule-surface interactions play therein, compared to the molecule-molecule interactions? In this paper, we employ all-atom MD simulations to investigate the influence of the local molecular dipole density on the nucleation and growth of the p -6P and its symmetrically fluorinated derivative p -6P4F on the a -SiO₂ surface. We simulate the growth of up to three complete layers and characterize the layer structures and the molecule-surface interactions to detect the driving mechanisms that govern the nucleation and growth of these molecules.

First, we simulate the growth of the first monolayer and analyze the average height, surface roughness and average layer inclination as a function of the surface density of the deposited molecules. We continue the study by depositing molecules onto the first layer and observe and analyze the formation of the second and third monolayers. We provide insight into the surface diffusion dynamics and calculate the binding energies of the molecule to the underlying layers. Finally, we measure the unit-cell parameters of the grown crystalline layers. We find that, before each layer is completed, the molecules in the first clusters form fan-like structures with gradually increasing inclination angles, if the molecule-surface interactions are strong enough compared to the molecule-molecule interactions. Eventually, some of the molecules in the fan-like structures are standing. Once the molecule-surface interactions become too weak, as it happens with the p -6P in the second monolayer but not with the p -6P4F, the inclination angle of the already standing molecules propagates through all deposited molecules, long before the layer is completed. When all molecules are standing, the energy barrier for single molecules to diffuse over the mound terraces becomes prohibitive. We finally propose this mechanism as the reason for the 3D mound growth in the case of p -6P in contrast to the smooth layer-by-layer growth of p -6P4F.

II. METHODS

A. Molecular models and simulation details

We perform classical, all-atom MD simulations using the GROMACS simulation package (version 5.1) [33]. The

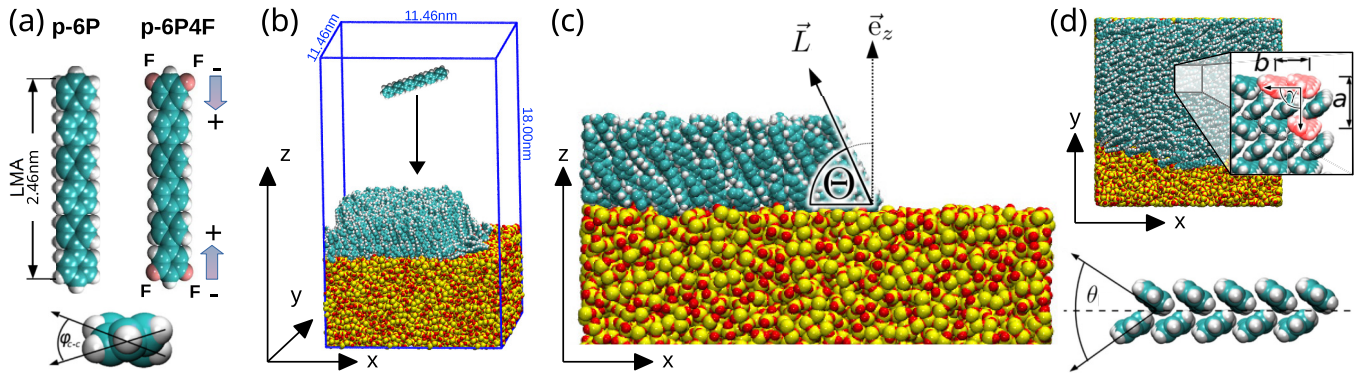


FIG. 1. Illustrations of the simulation setup, the molecules of interest, and important structural and crystallographic parameters. (a) The conjugated organic paraxiphenyl molecule (p -6P) and its fluorinated derivative p -6P4F. The long molecular axis (LMA) is defined as the axis which runs through both terminal carbons of the molecule. The fluorination introduces local dipole moments at the two head groups of the p -6P4F molecule. For a detailed distinction between the two molecules see Ref. [5]. The front view illustrates the torsional angle φ_{C-C} between neighboring phenyl rings. (b) The simulation setup for the deposition simulations. (c) Projection of the simulation box onto the x - z axis. The angle Θ , between the vector \vec{L} and the inorganic surface plane, describes the inclination of the molecules in the grown molecular layer [see Eq. (3)]. The vector \vec{L} is a vector parallel to the LMA of the molecules. The surface plane is defined by the unit vector in the direction of the z -axis \vec{e}_z . (d) Projection of the simulation box onto the x - y axis. The inset shows a schematic illustration of the lattice parameters a , b and the monoclinic angle γ between the crystallographic a - and b -axes. The grown molecular layers possess a herringbone structure with the herringbone-angle θ between the molecular planes of the two molecules of each base.

simulation setup is illustrated in Fig. 1. The atomic configuration of an α -SiO₂ slab was exported from the VMD molecular visualization software using the INORGANIC BUILDER tool [34]. The slab with dimensions $11.46 \times 11.46 \times 5.67$ nm³ was equilibrated for 5 ns, with a time step of 0.002 ps, in contact with a heat bath at 300 K. The simulation involved 15 488 Si and 30 976 O atoms maintained at the bulk density of 2.18 g/cm³, in agreement with the experimental density of 2.20 g/cm³ [35]. Corresponding radial distribution functions for Si-Si, O-O, and Si-O atom pairs [36] are in agreement with the x-ray diffraction experiments [35] and MD simulation results from Ref. [37]. The interatomic interactions within the α -SiO₂ are modelled by Lennard-Jones (LJ) and Coulomb interactions to account for van der Waals and electrostatic interactions, respectively. The partial charges placed on the individual Si and O atoms together with the LJ potential parameters are taken from Ref. [38]. To simulate the molecular self-assembly on inorganic surfaces, there is a requirement on the force field to reproduce the correct organic-organic as well as inorganic-organic interactions. We previously proposed a force field that is capable of providing a spontaneously self-assembled room-temperature solid p -6P bulk crystal with unit-cell parameters in agreement with experimental measurements [39]. For modeling the intramolecular and LJ interactions of the p -6P and p -6P4F molecules, the generalized Amber force field [40] is employed. The atomic partial charges were calculated with the GAUSSIAN 09 SOFTWARE [41] using the B3LYP functional and the cc-pVTZ basis set with the electrostatic potential fit method [42]. For p -6P, the LJ parameters and partial charges are the same as used in Ref. [39], and for the p -6P4F molecule they are the same as in Ref. [5]. Maps of the partial charge distributions in both molecules are provided in the Supplemental Material [43]. The differences between the two molecules in respect to their dipole densities are discussed in Ref. [5] in detail. The LJ interactions between the molecules

and the α -SiO₂ surface are governed by the Lorentz-Berthelot combination rules.

To ensure an adequate sampling of the phase space, the time evolution of the position \vec{r}_i of each atom i is described by the Langevin equation of motion

$$m_i \frac{d^2 \vec{r}_i}{dt^2} = -m_i \xi_i \frac{d\vec{r}_i}{dt} + \vec{F}_i + \vec{R}_i, \quad (1)$$

where m_i is the atomic mass, ξ_i is the friction constant in units of ps⁻¹, \vec{F}_i is the force acting on atom i due to all other atoms, and $\vec{R}_i(t)$ is the random force obeying the fluctuation-dissipation theorem [44]. The equation of motion is integrated using a leapfrog algorithm with a time step of 2 fs. The long-range Coulomb interactions in the system are computed by the Particle Mesh Ewald method [44], using a Coulomb cutoff distance of 1 nm with interpolation order 4 and $30 \times 20 \times 35$ grid points in the x -, y -, and z -directions. For the LJ interactions a cutoff of 1.3 nm was applied.

Atoms in the bottom layer of the surface of thickness 1 nm were simulated fixed to their initial relaxed positions to serve as a structural template for the thermalized α -SiO₂ surface. The simulation box was enlarged in the z -direction, creating an empty region where molecules can be inserted, with a final box size of $11.46 \times 11.46 \times 18.00$ nm³ and periodic boundary conditions only applied in the x - and y -directions.

B. Simulation of the experimental deposition process

The experimental deposition process is simulated as follows. After an equilibration simulation of the bare α -SiO₂ surface, a single molecule is inserted into the top of the simulation box. The initial orientation and position of the molecule are random, albeit restricted to the top of the box such that the distance between the newly inserted molecule's atoms and the rest of the system is at least 5 nm. At the start of the simulation, the molecule is accelerated in the negative

z -direction [towards the surface, see Fig. 1(b)]. After a certain time τ_{in} , the acceleration is removed from the molecule and a new molecule is inserted, again with a random yet restricted orientation and position and with a downwards acceleration. This process is repeated until three full monolayers have formed.

The time τ_{in} between two consecutive insertions is restricted due to the computational cost associated with the necessary lengthscales. If possible, e.g., during the growth of the first monolayer, we set $\tau_{\text{in}} = 3000$ ps (corresponding to the deposition rate τ_{in}^{-1}). When more molecules are involved, we use $\tau_{\text{in}} = 300$ ps, which corresponds to a higher deposition rate. We also investigate what happens if $\tau_{\text{in}} = 30$ ps. We note that it is not straightforward to compare our deposition rates to experimental rates since, in experiments, the surfaces are much bigger than ours. Potocar *et al.* [45], for instance, deposited p -6P on a 1 cm^2 mica surface with a flux of $1.47 \times 10^{-15} \text{ nm}^{-2} \times \text{ps}^{-1}$. This is approx. 1.7×10^9 times slower than we do in our simulations with the slowest rate ($3000^{-1} \text{ ps}^{-1}$ translates to $2.54 \times 10^{-6} \text{ nm}^{-2} \times \text{ps}^{-1}$). However, on bigger surfaces the molecules do not spread homogeneously, but move collectively towards few molecular islands. This increases the effective growth rate per island again in a complicated fashion. Our rates are comparable with previous simulations of pentacene deposition on α -SiO₂ [18]. As for the computational cost, we simulate on the neuroscience, elementary particle physics, microsystems engineering, and materials science (NEMO) cluster of Freiburg University using 160 cores, and the core hours per ns amount to 85.635 h/ns.

The small acceleration that every newly inserted molecule is exposed to is necessary to slowly bring the molecule within range of the molecule-surface interactions. If $\tau_{\text{in}} = 3000$ ps, we have enough time to accelerate relatively slowly ($a_z = -0.01 \text{ nm/ps}^2$). In the simulations with $\tau_{\text{in}} = 300$ ps and $\tau_{\text{in}} = 30$ ps, the acceleration has to be increased to $a_z = -0.03 \text{ nm/ps}^2$ and $a_z = -0.05 \text{ nm/ps}^2$, respectively.

The deposition simulation is performed at a temperature of 575 K. This temperature is higher than those usually employed in deposition experiments [46]. However, it was shown that, at this temperature in our model, bulk crystals from p -6P molecules exhibit a well-ordered room-temperature-like smectic-C phase with the correct herringbone and inclination angles [39]. The inclination angle becomes zero at 590 K where a transition from the smectic-C to the smectic-B phase occurs. We thus adopt a relatively high temperature in our simulations to speed up the molecular motion to prevent molecules from getting kinetically trapped due to the high (compared to experiments) deposition rate [47]. If the deposition simulation is directly performed at $T = 300$ K, the molecules self-assemble into irregular structures and layer-by-layer growth is no longer observed. Yet, by gradual temperature annealing from $T = 575$ K to $T = 300$ K we can equilibrate the final structures into the correct room-temperature crystal structure.

C. Single molecule surface binding

To interpret the structures of the grown molecular layers, it is imperative to know the free energy for the

binding/unbinding process, ΔF_b , of a molecule to its substrate [31]. We thus calculate ΔF_b between a single p -6P molecule and the bare α -SiO₂ surface, a surface comprised of a single molecular layer of p -6P molecules, and a surface comprised of two layers of p -6P molecules. We do the same for the p -6P4F molecule with α -SiO₂ and p -6P4F layers as surfaces. The surfaces are taken from the simulations described in the previous section.

ΔF_b is estimated from the potentials of mean force (PMF) as $\Delta F_b = F_b(z_0) - F_b(z_{\text{max}})$ where z_0 and z_{max} are the global minimum of the curve and the reference distance along the z coordinate, respectively. The reference distance z_{max} is defined as the distance between molecule and surface where both are so far apart that they do not exert influence on each other. The PMFs are calculated from steered MD simulations [33] at $T = 575$ K, where the center of mass (COM) of the molecule is connected to a virtual site via a harmonic potential with the spring constant $k = 5000 \text{ kJ mol}^{-1} \text{ nm}^{-1}$, while the virtual site moves away from the surface with a constant velocity of $10^{-4} \text{ nm ps}^{-1}$. We pull for 5×10^5 ps. The chosen value for the pulling velocity is lower by at least a factor of 5 compared to previously employed pulling velocities in studies of binding of structurally similar or more complex ligands to protein structures [48,49]. It was found to be a good compromise between the accuracy and the simulation speed. The PMF is then obtained from the integral of the net force acting on the harmonic spring while the molecule is pulled away from the surface. The origin $z = 0$ is defined as the z -coordinate of the highest atom of the α -SiO₂ surface.

D. Surface diffusion

While molecules are deposited one by one on the surface, each molecule diffuses on the surface before it eventually integrates into a molecular cluster. Thus, understanding the subtle differences in diffusion between the p -6P and p -6P4F can help us to understand the differences in their growth modes. The total long-time in-plane diffusion coefficients D^{tot} averaged over the x - and y -directions of the molecular motion, are obtained from the mean squared displacements (MSDs) of the molecular COM from simulations via

$$\langle [x(t) - x(t_0)]^2 + [y(t) - y(t_0)]^2 \rangle = \lim_{t \rightarrow \infty} 4D^{\text{tot}}t, \quad (2)$$

where $x(t)$ and $y(t)$ are the coordinates of the molecular COM at time t and $\langle \rangle$ denotes the ensemble average. Due to the limits imposed on the diffusion by the bath friction from the Langevin equation, D^{tot} slightly underestimates the real diffusion coefficient, as discussed in Ref. [36]. For easier understanding, the details of the diffusion simulations are given in the discussion, see Sec. III D.

III. RESULTS

A. Formation of the first monolayer

In this section we examine the influence of change in molecular polarity on the formation and structural properties of the first monolayer (1ML). The deposition simulation is performed by inserting one molecule into the simulation box every 3000 ps (that corresponds to a rate of $3000^{-1} \text{ ps}^{-1}$).

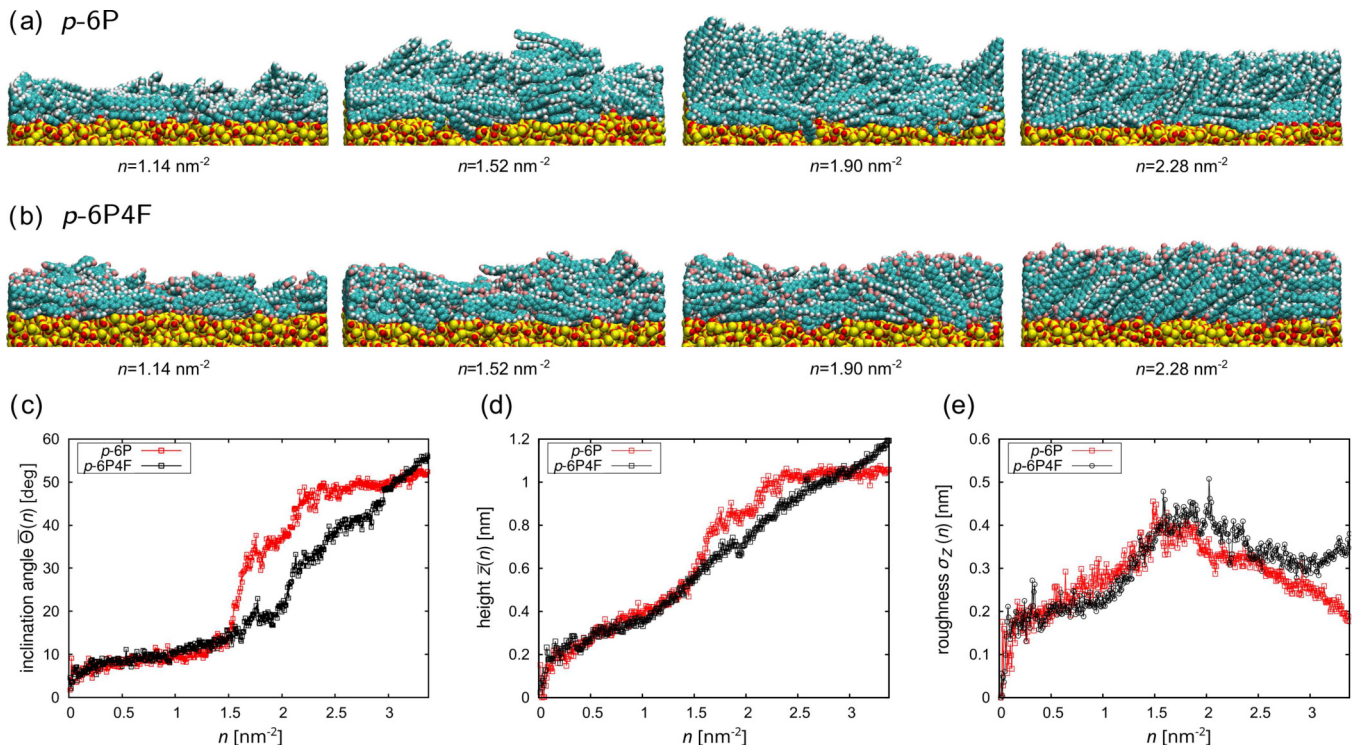


FIG. 2. (a) Simulation snapshots of p -6P molecules deposited onto the α -SiO₂ surface, at $T = 575$ K with a deposition rate of 3000^{-1} ps⁻¹. (b) Simulation snapshots of p -6P4F molecules deposited onto the α -SiO₂ surface, at $T = 575$ K with a deposition rate of 3000^{-1} ps⁻¹. (c) The average inclination angle $\bar{\Theta}(n)$ [Eq. (3)] of the IML as a function of the surface density n of the deposited p -6P and p -6P4F molecules. (d) The average height $\bar{z}(n)$ [Eq. (4)] of the center of mass of the IML. (e) The roughness $\sigma_z(n)$ [Eq. (5)] of the IML.

In Figs. 2(a) and 2(b) we show simulation snapshots for the p -6P and p -6P4F molecules. Fig. 2(c) shows the average inclination angle $\bar{\Theta}(n)$ as a function of the surface density n , which is defined as the number of already deposited molecules N divided by the area of the surface (11.46×11.46 nm²). The inclination angle $\Theta_i(n)$ of a single molecule i is defined as the angle between the LMA and the surface plane via

$$\Theta_i(n) = \arcsin\left(\frac{\vec{L}_i(n) \cdot \vec{e}_z}{|\vec{L}_i(n)|}\right), \quad (3)$$

where $\vec{L}_i(n)$ is a vector parallel to the long molecular axis (LMA), pointing from one terminal carbon of the molecule i to the other. The surface normal is described by \vec{e}_z , which is the unit vector in the direction of the z -axis. The average inclination angle is calculated from the arithmetic average of the sine of the angles by $\bar{\Theta}(n) = \arcsin(\overline{\sin[\Theta_i(n)]})$. Figure 2(d) shows the average height $\bar{z}(n) = 1/N \sum_i z_i(n)$ of the COM of the IML as a function of surface density n , where the COM height of a molecule i ,

$$z_i(n) = z_i^{\text{COM}}(n) - z^{\alpha\text{-SiO}_2} \quad (4)$$

is the difference between the z -coordinate of the molecule's COM and the z -coordinate of the highest atom of the α -SiO₂ surface.

Finally, Fig. 2(e) shows the roughness $\sigma_z(n)$ of the IML, calculated as the standard deviation of the IML COM

height

$$\sigma_z(n) = \sqrt{\frac{1}{N-1} \sum_i [z_i(n) - \bar{z}(n)]^2}. \quad (5)$$

Up until the first 150 molecules are deposited (corresponding to a surface area density of $n = 1.14$ nm⁻²), all molecules are lying flat on the surface. At this stage, the molecules resemble a molecular liquid and homogeneously wet the surface. However, as molecules slide over each other, they start to create fan-like structures, where each consecutive molecule has a higher angle because it is partly propped by other molecules lying underneath. This can be nicely observed in the $n = 1.52$ nm⁻² snapshot for the case of p -6P or in the $n = 1.90$ nm⁻² snapshot in the case of p -6P4F, for example. Since these molecules are not only tilted in respect to the surface but also in respect to each other, the clusters resemble a layer of a chiral liquid crystal, where the molecules twist around the layer normal. The chirality of the clusters correlates with the inclination angle of the molecules, but it is only the gradual fan-like increase of this angle that facilitates the upright standing growth of the molecules. The more molecules are integrated into these chiral fans, the more molecules will eventually be standing instead of lying, and the average inclination angle of the IML increases [see Fig. 2(c)]. This process culminates in an abrupt unbinding of the molecules from the surface while they instead bind to the already standing molecules. It is a common observation in simulations and experiments that the switch

from a layer of mostly lying to a layer of standing molecules occurs collectively and quickly, but only once a critical coverage is reached [18,31,45]. After about 400 molecules are deposited on the surface (corresponding to a surface area density of $n = 3.04 \text{ nm}^{-2}$), almost all the molecules of the 1ML are standing and the average COM height approaches $z \approx 1.2 \text{ nm}$ [see Fig. 2(d)]. The second monolayer then starts forming at $n \approx 3.8 \text{ nm}^{-2}$, after the 1ML is completed. The density of the 1ML is comparable to experimental values of *p*-6P grown on amorphous mica (4.4 nm^{-2}) [45].

At a glance, the growth of the 1ML seems to proceed very similarly for both molecules. However, the average inclination angle and height of the 1ML [Figs. 2(c) and 2(d)] behave differently for the two molecules at $n > 1.5 \text{ nm}^{-2}$. First, the abrupt change of the inclination happens at a lower surface density for *p*-6P than for *p*-6P4F. Second, the inclination and height show a plateau behavior in the case of *p*-6P, but a monotonic increase in the case of *p*-6P4F. The first point is discussed in the next paragraph. Regarding the second point, it is not clear whether the different behavior is due to statistical fluctuations or an actual effect of the fluorination. As we will observe during the growth of the second layer, there both molecules will run into a plateau in respect to the inclination while the height will increase monotonically. A closer inspection of the trajectories reveals that the inclination angle of the *p*-6P4F 1ML still fluctuates while the first molecules of the second layer fall onto the 1ML. At the same time, the inclination angle of the *p*-6P 1ML seems to have already equilibrated. One possibility to explain this is that due to the additional strong dipoles of the *p*-6P4F, it just takes a longer time for the molecules to equilibrate into a final structure. The roughness of the 1ML increases as molecules are deposited on the surface and as the amount of chiral structures increases [see Fig. 2(e)]. The roughness reaches its peak above $n = 1.5 \text{ nm}^{-2}$ when the orientational change propagates through the 1ML and decreases after $n \approx 2 \text{ nm}^{-2}$, where the chiral structures are replaced by regular crystallinity, in both cases.

Figure 3 shows number density profiles of the molecular COMs as a function of height z and surface density n for the *p*-6P and *p*-6P4F. The peak of the red curve (*p*-6P) progresses faster along the z -axis with increasing n compared to the black curve (*p*-6P4F), indicating that the *p*-6P changes the orientation sooner compared to the fluorinated molecule. Due to the polar head and tail groups in the *p*-6P4F, the fluorinated molecules bind stronger to the *a*-SiO₂ surface, which delays their reorientation. This result, based on a single deposition simulation, could also indicate that the *p*-6P requires a smaller critical nucleus size to have an orientational change. However, additional deposition simulations are required to support this conclusion.

B. Formation of the second monolayer

In this section we examine the influence of change in molecular polarity on the formation and structural properties of two monolayers. Due to the increase in the computational cost with an increase in the system size, we have to simulate the growth of the layers with a faster rate of 300^{-1} ps^{-1} . The consequences of this choice are discussed in the Supplemental Material [43]. The deposition of both *p*-6P4F and *p*-6P leads

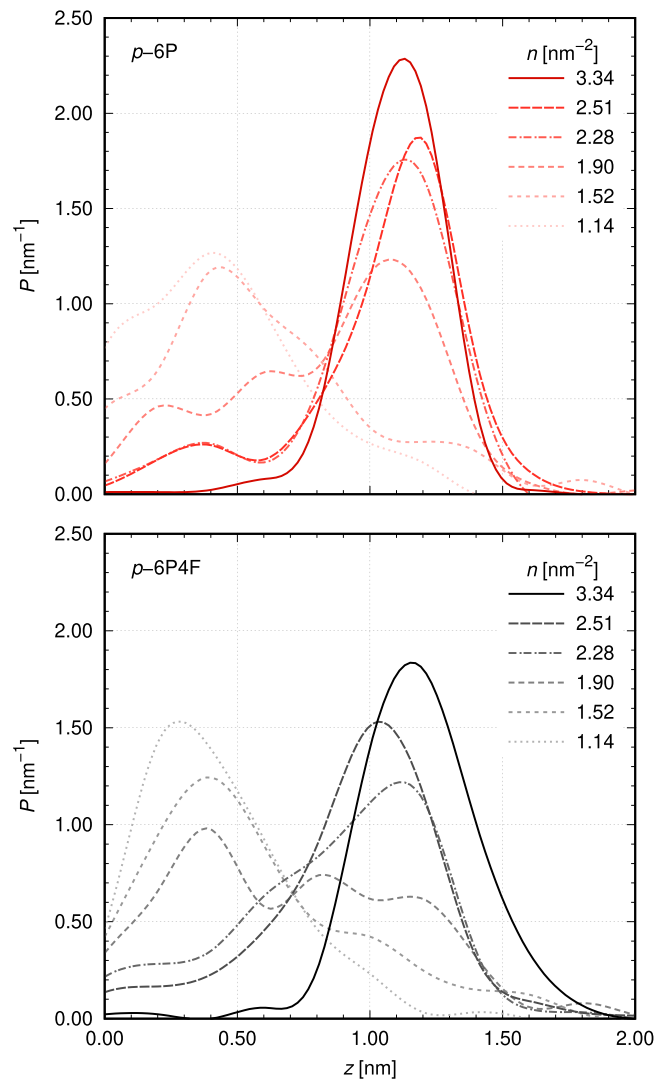


FIG. 3. Normalized number density profiles of the molecular COMs as a function of height z for the *p*-6P and *p*-6P4F molecules deposited onto the *a*-SiO₂ surface with a deposition rate of $3000^{-1} \text{ ps}^{-1}$. The lines correspond to different surface densities n of the deposited molecules. The average COM z -coordinate of 1.23 nm equals half of the molecular length (corresponding to molecules in the upright standing configuration).

to the formation of a crystalline 1ML with standing and tilted molecules, in accordance with experiments [7] and with our simulations of the 1ML at a lower rate in the previous section. Figures 4(a) and 4(b) show representative snapshots of the second and third monolayers consisting of the (a) *p*-6P and (b) *p*-6P4F.

In the second monolayer (2ML), smooth, layer-by-layer growth is observed in the case of *p*-6P4F. First, the molecules form big chiral structures with different inclination angles, sometimes also resembling wooden logs arranged in a campfire [see Fig. 4(f)]. Such supramolecular assemblies were reported in simulations of sexithiophene on C₆₀ [19]. The process is very similar to the growth of the 1ML with the difference that the molecules start to form the chiral structures on the 2ML at a much lower surface coverage compared to

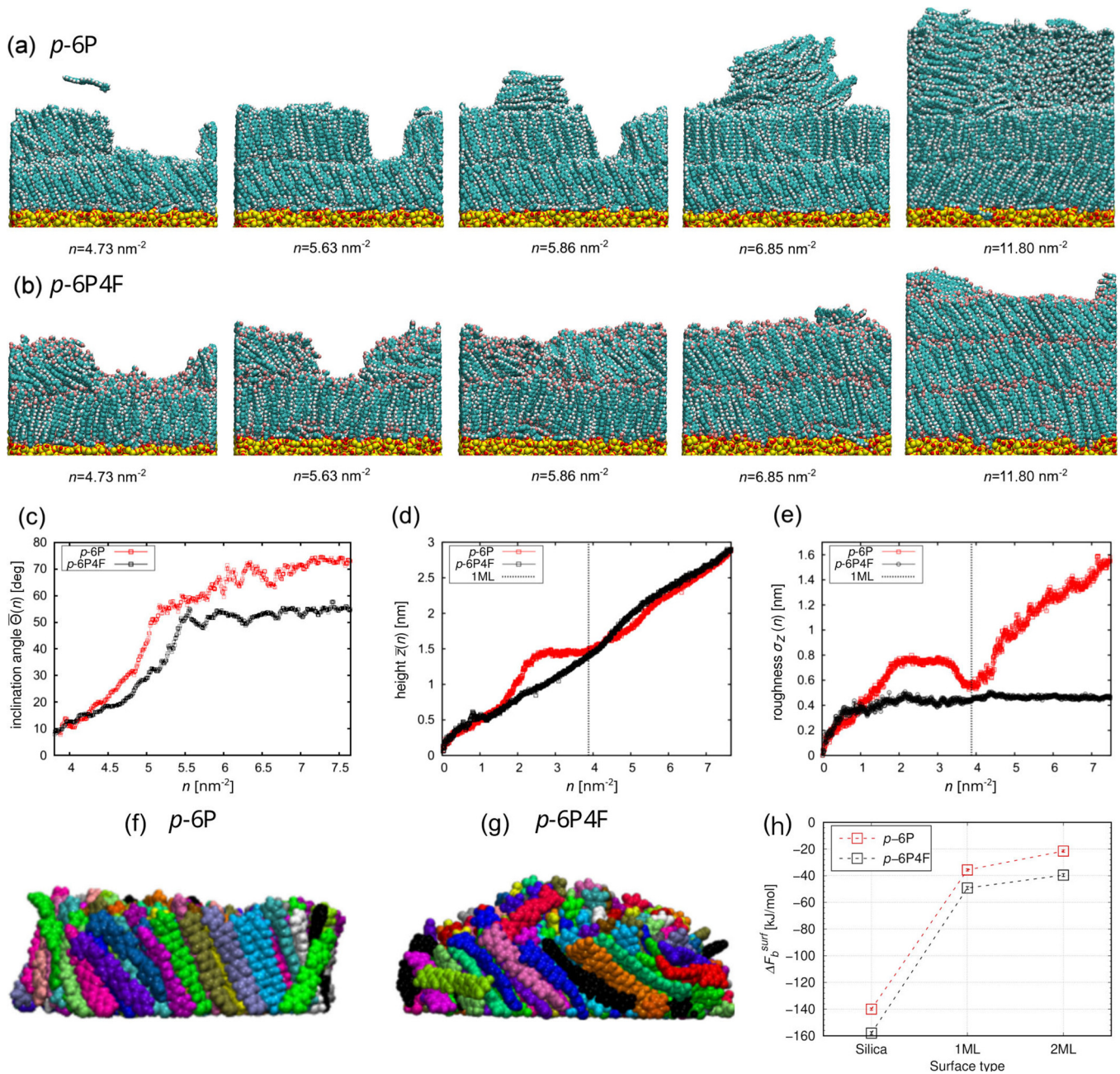


FIG. 4. (a) Simulation snapshots of *p*-6P molecules deposited onto the *a*-SiO₂ surface, at $T = 575$ K with a deposition rate of 300^{-1} ps⁻¹. The number of molecules increases from 600 to 1500 from left to right. (b) Simulation snapshots of *p*-6P4F molecules deposited onto the *a*-SiO₂ surface, at $T = 575$ K with a deposition rate of 300^{-1} ps⁻¹. As in the case of the *p*-6P, the number of molecules increases from 600 to 1500 from left to right. (c) The average inclination angle $\bar{\Theta}(n)$ [Eq. (3)] of the deposited layers as a function of the surface density n of the deposited *p*-6P and *p*-6P4F molecules. (d) The average height $\bar{z}(n)$ [Eq. (4)] of the center of mass of the deposited layers. (e) The roughness $\sigma_z(n)$ [Eq. (5)] of the deposited layers. (f)–(g) Side view of the chiral crystalline islands formed by the *p*-6P and *p*-6P4F molecules adsorbed on the respective 1MLs, with surface densities of $n = 5.10$ nm⁻². For clarity the 1ML and *a*-SiO₂ substrates are not shown and molecules are drawn with different colors. (h) Comparison of the binding free energy of the *p*-6P and *p*-6P4F molecules at $T = 575$ K to three different surfaces: *a*-SiO₂, 1ML, and 2ML.

the 1ML growth on bare *a*-SiO₂. This is because, in contrast to the growth of the 1ML on *a*-SiO₂, the molecules do not wet the entire surface before clustering into fan-like clusters that eventually lead to the first standing molecules. Instead, the *p*-6P4F molecules form the fan-like clusters very soon after being deposited [see Fig. 4(g)]. Previous simulation studies already showed that a higher attraction between molecule

and substrate causes the transition from lying to standing to occur at higher coverages and vice versa [31,45]. In our case, the attraction between the molecule and its 1ML surface is much weaker than the attraction between the molecule and the *a*-SiO₂ surface. Figure 4(h) compares the binding free energies on three different surfaces onto which molecules are deposited: *a*-SiO₂, 1ML, and 2ML. We find that the surface

binding free energy decreases with each new monolayer. Beyond that, the 2ML grows just like the 1ML did: Once the clusters become big enough, the number of upright standing molecules increases until it becomes energetically favorable for the other molecules to stand up as well. After the 2ML is completed, the 3ML proceeds to grow in the same way as the 2ML.

In the case of the p -6P, we observe a different behavior during the growth of the 2ML. After 50 molecules are deposited, the first clusters grow similarly to p -6P4F: they form chiral structures. However, the 2ML loses its chiral property at a much lower coverage than it does in the p -6P4F case, as can be seen in Fig. 5, which shows probability distributions of the (cosine of the) inclination angle of the molecules belonging to the 2ML. At a surface coverage of 5.63 nm^{-2} , i.e., before the 2ML is complete, most p -6P molecules are already standing. This is because p -6P binds weaker to its underlying 1ML surface than the p -6P4F [see Fig. 4(h)]. Generally, the p -6P4F binds stronger to the a -SiO₂ surface, 1ML and 2ML than the p -6P. The stronger binding is a consequence of the polar head and tail groups in the p -6P4F interacting with local surface dipoles.

From then on, in the 3ML, p -6P grows into irregular structures, which was previously observed in growth experiments of p -6P on the ZnO (10 $\bar{1}$ 0) surface [7]. As shown in the central snapshot in Fig. 4(a), the newly deposited molecules that get adsorbed on the top of the 2ML do not diffuse down the step-edge to integrate into the 2ML, but form new clusters which are no longer chiral. They form stacks of equally oriented, lying molecules which only grow bigger in size when more molecules are adsorbed. Eventually, the 2ML gets filled with those molecules that are, by chance, inserted into the simulation box right above the gap of the 2ML. The gap does not get filled by molecules diffusing down from the top of the 2ML, as was previously observed [50]. By that time, the cluster on top of the 2ML has grown significantly, causing a strong increase of the roughness [see Fig. 4(d)]. A similar behavior of the roughness was observed in experiments [7]. Within the simulation time, those clusters do not change their orientation. Thus, what should essentially be the 3ML instead becomes a structure of lying molecules, growing vertically.

Chirality at the edges of the p -6P4F islands facilitates downward mass transport and conversely, layer-by-layer growth. Because of the quite diverse morphology of the chiral terrace step-edge and the relatively small inclination angles of the step-edge molecules, the diffusing molecules have a relatively high chance to find an energy pathway low enough for them to descend the p -6P4F step edge and integrate into the existing layer. It was shown that the barrier for the terrace crossing strongly depends on the average inclination of the island and decreases with a decrease in the inclination angle [50]. Based on the results shown in Fig. 5, the average inclination of the p -6P4F islands is lower compared to the p -6P for the same surface density. However, in the case of the p -6P, weaker attraction to the surface enhances both the diffusivity and cluster formation, but reduces the chirality at the island edges. There is a threshold surface density where this effect becomes especially prominent, which is between $n = 5.10$ and 5.55 nm^{-2} , with an average island inclination angle of around 76° . Thus, with less-inclined islands, where

TABLE I. Diffusion coefficients $D^{\text{tot}}(T)$ in units of $\text{nm}^2\text{ps}^{-1}$ calculated according to Eq. (2) for single p -6P and p -6P4F molecules diffusing on the a -SiO₂ and 1ML at $T = 575 \text{ K}$.

T (K)	On a -SiO ₂		On 1ML	
	p -6P	p -6P4F	p -6P	p -6P4F
575	1.19×10^{-4} $\pm 2 \times 10^{-5}$	1.11×10^{-4} $\pm 3 \times 10^{-5}$	6.13×10^{-3} $\pm 2 \times 10^{-6}$	3.91×10^{-3} $\pm 3 \times 10^{-6}$

the chirality is significantly reduced at the island edges at the surface densities $n \geq 5.55 \text{ nm}^{-2}$, p -6P experiences higher a barrier for the terrace crossing compared the p -6P4F, which hampers layer-by-layer growth starting from the 2ML.

C. Interface layers

We also observe the presence of horizontal molecules between the a -SiO₂ surface and the 1ML, that belong to the interface layer (IL). The existence of one or several ILs or wetting layers of flat molecules was reported in several studies for molecules such as p -6P, pentacene, anthracene, and rubicene [18,48,51,52] where, in some cases, the insertion of organic ILs was utilized as a technique to passivate or manipulate the interaction with metallic surfaces. In our case, the number of molecules that belong to the interface layer increases with an increase in the number of polar groups in the molecule and amounts to three and eight molecules for the p -6P and p -6P4F in the 1ML, respectively, while the 2ML proceeds to grow without an IL. This might be a consequence of the stronger interaction of the molecules with a -SiO₂ compared to their respective 1MLs [see Fig. 4(h)]. However, as the ILs in this case are characterized each based on a single deposition simulation, our result can provide an inspiration for studying ILs from multiple deposition simulations for statistically meaningful results.

Some molecules belonging to the IL are able to diffuse on the bare surface but become kinetically trapped below the growing 1ML terrace, while some others are immobile on specific positions on the a -SiO₂ surface. As it was previously suggested that these immobile IL molecules could play a role in the formation of the 1ML on a -SiO₂ [18], it is important to study how the single molecule surface diffusion is related to the formation of ILs.

D. Single molecule surface diffusion

When in equilibrium, single molecules are observed to adsorb and diffuse in a flat-lying geometry on the surface. To study the surface diffusion, we simulate (i) a single p -6P molecule on the bare a -SiO₂ surface, (ii) a single p -6P4F molecule on the bare a -SiO₂ surface, (iii) a single p -6P molecule on top of the 1ML made of p -6P molecules, and (iv) a single p -6P4F molecule on top of the 1ML made of p -6P4F molecules. The investigated temperatures are $T = 600, 610, 640, \text{ and } 650 \text{ K}$. The diffusion coefficients are calculated according to Eq. (2). The T -dependent diffusion coefficients and resulting diffusion energy barriers are discussed in the Supplemental Material [43].

Here, we present in Table I the results for $T = 575 \text{ K}$, which are extrapolated using the Arrhenius equation (see Sup-

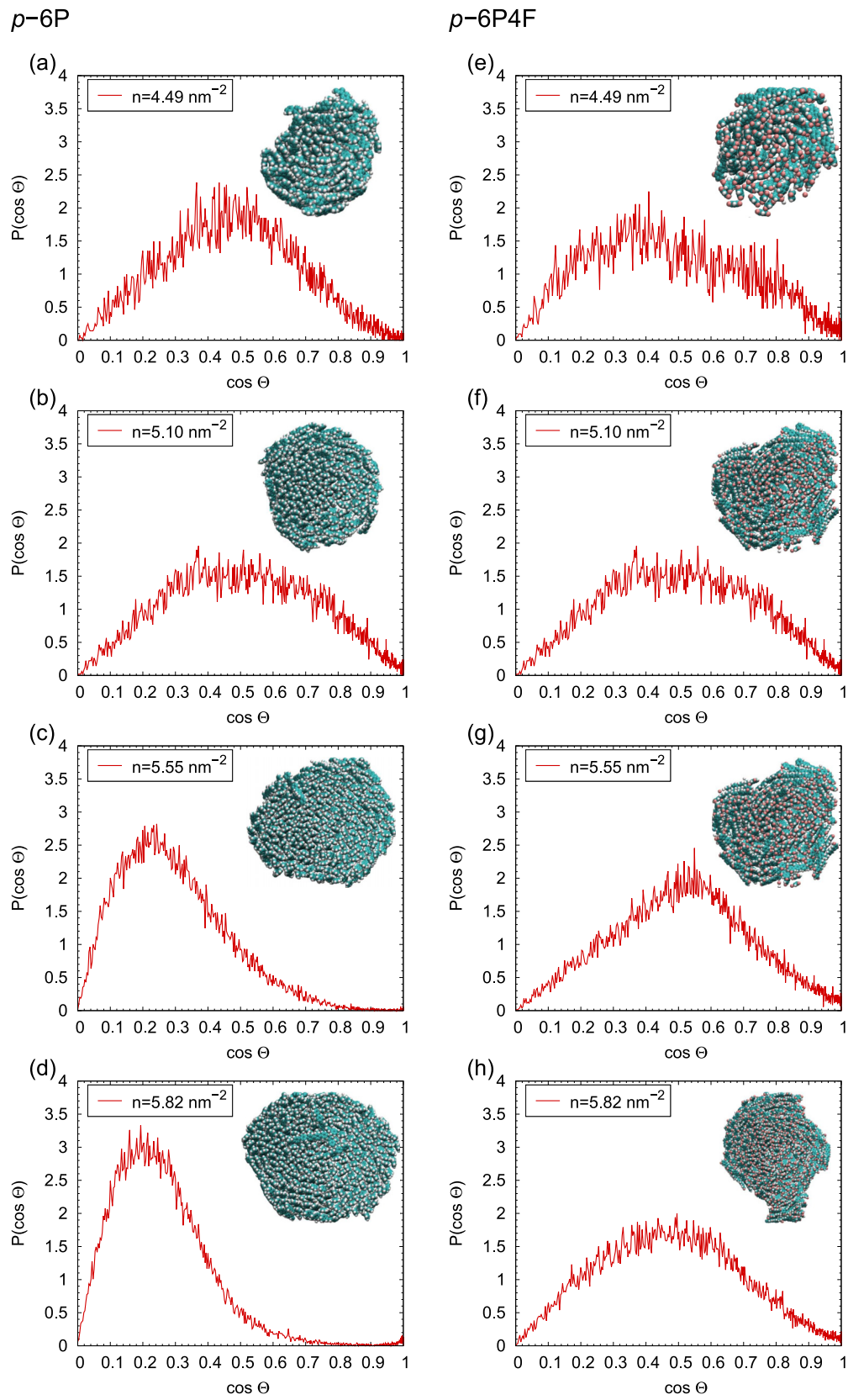


FIG. 5. Probability distributions of the (cosine of the) inclination angle for the molecules in the 2ML. The insets of the figures are showing representative snapshots of grown islands observed from the top, displaying the chiral island edges.

TABLE II. Calculated room-temperature (herringbone-phase) properties of the p -6P and p -6P4F 1ML and 2ML structures. Obtained results are compared with the p -6P bulk crystal structure properties at $T = 300$ K from MD simulations [39] and experimental [53] studies. The unit-cell parameters a , b , γ ; the herringbone angle θ ; inclination angle Θ ; and torsion angle φ_{c-c} are defined in Fig. 1. ρ is the mass density of the molecules.

			a [nm]	b [nm]	γ [°]	θ [°]	Θ [°]	φ_{c-c} [°]	ρ [g/cm ³]
Present study	1ML	p -6P	0.95 ± 0.17	0.54 ± 0.04	90.08 ± 13.30	64.30 ± 19.40	52.22 ± 14.00	15.40 ± 11.00	1.31 ± 0.07
		p -6P4F	1.00 ± 0.06	0.50 ± 0.05	91.9 ± 16.50	75.70 ± 25.10	55.02 ± 13.50	18.30 ± 11.50	1.31 ± 0.07
	2ML	p -6P	0.86 ± 0.06	0.56 ± 0.03	91.50 ± 6.30	57.30 ± 14.9	61.66 ± 22.00	13.80 ± 9.70	1.33 ± 0.06
		p -6P4F	0.97 ± 0.08	0.51 ± 0.06	81.60 ± 18.5	62.00 ± 18.50	52.06 ± 22.00	17.00 ± 10.70	1.31 ± 0.09
Literature	bulk	p -6P [39]	0.827 ± 0.01	0.548 ± 0.01	89.80 ± 3.30	61.7 ± 13.70	72.30 ± 6.00	15.70 ± 7.90	1.29 ± 0.02
		p -6P [53]	0.809	0.557	90.00	66.00	72.00	20.00	1.30
	1ML	p -6P4F [7]	n/a	n/a	n/a	n/a	76	n/a	n/a
	2ML	p -6P4F [7]	n/a	n/a	n/a	n/a	65	n/a	n/a

plemental Material [43]). As we can observe, on α -SiO₂, the p -6P4F has a lower diffusion coefficient compared to the p -6P. This result indicates that p -6P4F molecules are more likely to become trapped at the IL during the deposition. On the 1ML, the p -6P also diffuses faster than the p -6P4F. Finally, we see that the diffusion coefficients of both molecules on the 1ML are about one order of magnitude higher compared to the diffusion coefficients on α -SiO₂. This result supports our finding that, once the 1ML is finished, the orientational change during the 2ML growth happens sooner as molecules diffuse significantly faster than on the bare α -SiO₂ and are able to find their binding partners sooner in the given simulation time. It is also consistent with the binding free energies in Fig. 4(h). The stronger molecule-surface attraction of the p -6P4F, due to the polar groups, hampers the diffusion on α -SiO₂ and also on the 1ML and 2ML. This also increases the number of molecules participating in the IL.

The average timescale for the diffusion process to be activated on the surfaces is about 1 ns on average [36]. This suggests that one should refer to the system-specific diffusion timescale while opting for a deposition rate in the MD simulations of growth. Note that, in our simulations, the deposition time scale of $\tau_{in} = 3000$ ps is three times higher than the average diffusion timescale.

E. Structural properties of adsorbed layers

1. Structural properties of the 1ML

After the completion of the 1ML, the final structure is equilibrated with temperature annealing by decreasing the system temperature gradually from $T = 575$ K to $T = 300$ K. Table II (1ML) is showing the room-temperature (herringbone-phase) properties of the final p -6P and p -6P4F 1ML structures. In case of the p -6P, we can compare all structural properties in Table II to their respective bulk values obtained from previous MD simulations with the same model and from experiments. Unfortunately there exist, to the best of our knowledge, no experimental references for the p -6P4F unit-cell parameters. The only available data pertain to the heights of the first few MLs grown on the ZnO (10 $\bar{1}$ 0) surface, from which inclination angles can be deduced [7]. The measured layer heights for both molecules are separately compared to our simulations in Table III.

2. Structural properties of the 2ML

We further investigate the structural properties of the 2ML by quantifying unit-cell parameters. Table II (2ML) shows the room-temperature herringbone-phase properties of the p -6P and p -6P4F. After the completion of the 2ML, the final structure is equilibrated with gradual temperature annealing by decreasing the system temperature from $T = 575$ K to $T = 300$ K.

In the case of the p -6P, the 1ML and 2ML unit-cells are rotated around the z -axis relative to each other by 111° and in the case of the p -6P4F by 152° . A situation qualitatively similar to this was found for films grown from p -6P molecules that were fluorinated on one side only [8]. The adjacent layers were not in lateral registry with each other. This is, however, atypical for p -6P and p -6P4F molecules and might be an artifact of the relatively high deposition rate. The distances between the 1ML and the 2ML along the layer normal are reported in Table III.

The interactions between the equidirectional dipoles of adjacent p -6P4F molecules cause the molecules to distort so that the p -6P4F layer structure shows a lower level of structural ordering compared to the p -6P. The 1ML structure in both cases is less ordered compared to the 2ML structure, which comes as an effect of the interaction with the underlying α -SiO₂ surface and the molecules in the interface layer. Even though the molecules are packed in the bulk crystal structure, the complex interplay between the molecule-molecule and molecule- α -SiO₂ interactions decrease the degree of ordering in the case of the p -6P4F.

TABLE III. Heights of the respective MLs. The height of the 1ML is defined as the difference between the average z -coordinates of the topmost α -SiO₂ layer and the terminal H-atoms of the 1ML. The height of the 2ML is defined as the distance between terminal H-atoms of the 1ML and those of the 2ML. Compare to Fig. 8 of Ref. [7].

		Heights of layers [nm]	
		p -6P	p -6P4F
Present study	1ML	2.59 ± 0.13	2.80 ± 0.24
	2ML	2.54 ± 0.24	2.36 ± 0.42
Ref. [7]	1ML	2.6 ± 0.3	2.64 ± 0.12
	2ML	2.6 ± 0.3	2.46 ± 0.06

3. Substrate-induced phases

Even though the growth of organic structures is governed by processes occurring on timescales and lengthscales largely exceeding those accessible in our simulations, our high-rate and high-temperature deposition simulations can reproduce the layer-by-layer growth of the first MLs, resulting in a realistic molecular packing. The agreement of the 1ML and 2ML with the measured values in Table II is very good in all properties except for the inclination angle. However, the agreement is better in the 2ML than in the 1ML. This points to the occurrence of substrate induced phases (SIPs), which have a different structure from the bulk. Measurements show that SIPs can coexist with bulk phases but due to experimental limitations it is not clear if both phases coexist already from the first layer onwards or if the bulk phases only appear above a critical film thickness [16]. Our simulations point to the second one since we see a gradual change of the unit-cell parameters with increasing ML. For the *p*-6P4F molecule, this has been shown experimentally to be the case as well [7]. For *p*-6P, however, measurements seem to not find gradual transitions from thin film to the bulk structures [7,9–11]. For example, it was observed that the height of each individual *p*-6P layer grown on the ZnO (10 $\bar{1}$ 0) surface does not change with the number of layers, as depicted in Table III [7]. Interestingly, even though the inclination angles in our simulations are both underestimated and layer dependent, both *p*-6P layers have almost the same height. The differences in layer height that should exist due to the different inclination angles are compensated by the molecules in the interface layer and by the different van der Waals radii of the *a*-SiO₂ surface (for the 1ML) compared to the molecular surface (for the 2ML).

Our simulations can also be interpreted in a way consistent with Ref. [14]. Simulations of pentacene showed that the 1ML is the same whether it grows on a surface or in vacuum. In a previous work, we simulated that the inclination angle of a single ML of *p*-6P grown in a vacuum is 60°, which is very similar to the 1ML grown in this study [39]. Thus, the differences between the first few MLs and the bulk may not be influenced by the substrate alone, but also by the lack of other molecules or, more generally, by the difference in coordination between the 1ML and the bulk.

IV. CONCLUSION

In summary, we theoretically investigated the role of change in polarity on nucleation and growth of the *p*-6P

and its symmetrically fluorinated derivative, *p*-6P4F, on the *a*-SiO₂ surface. We simulated the experimental vapor deposition process with all-atom MD simulations, using three different deposition rates. The growth of up to three complete monolayers was reproduced and monitored with the help of observables such as average height, surface roughness, and average inclination angle as a function of time, together with the visual inspection of the grown structures. In both cases, we observed the orientational change from lying to upright standing configuration once a critical surface density was reached. During the formation of both the first and second monolayers, molecules tended to grow in chiral, fan-like, structures, where each consecutive molecule had a higher angle because it was propped by all the other molecules lying underneath. The growth of chiral islands was the main mechanism with which the growth of the *p*-6P4F proceeds in the third layer, while the *p*-6P, due to the lower interaction with the underlying substrate, grows into islands with a lower degree of chirality. This ultimately led to a lower barrier for step-edge crossing for the *p*-6P4F, as the molecules adsorbed on the top of the chiral, structurally diverse island, have more different pathways available to ascend the terrace than the *p*-6P on the *p*-6P island. Thus, *p*-6P4F molecules have a relatively high chance to find an energy pathway low enough for them to descend the step-edge and integrate into the existing layer. We also measured the room-temperature unit-cell parameters in the first two layers. Taking into account that our model was capable of reproducing the bulk crystal structure, the structures in the first two layers show differences in respect to the bulk, which can be attributed to the occurrence of substrate induced phases. An important implication of our findings is that partial fluorination of the *p*-6P molecule can significantly alter its growth behavior by modifying the rough, 3D growth into a smooth, 2D layer-by-layer growth in case of the *p*-6P4F. This has implications for the rational design of molecules and their functionalized forms which could be tailored for a desired growth behavior and HIOS structure formation.

ACKNOWLEDGMENTS

The study was funded by the Deutsche Forschungsgemeinschaft (DFG, German Research Foundation) under Project No. 182087777-SFB 951 (project A7). The authors wish to thank Sabine Klapp, Thomas Martynec, Stefan Kowarik, and Anton Zykov for inspiring discussions.

-
- [1] S. Blumstengel, S. Sadofev, and F. Henneberger, *New J. Phys.* **10**, 065010 (2008).
 - [2] N. Koch, *J. Phys.: Condens. Matter* **20**, 184008 (2008).
 - [3] T. Trevethan, A. Shluger, and L. Kantorovich, *J. Phys.: Condens. Matter* **22**, 084024 (2010).
 - [4] J. Niederhausen, Y. Zhang, F. Cheenicode Kabeer, Y. Garmshausen, B. M. Schmidt, Y. Li, K.-F. Braun, S. Hecht, A. Tkatchenko, N. Koch, and S.-W. Hla, *J. Phys. Chem. C* **122**, 18902 (2018).
 - [5] M. Miletic, K. Palczynski, M. R. Jacobs, A. M. Valencia, C. Cocchi, and J. Dzubiella, *J. Phys. Chem. C* **123**, 6549 (2019).
 - [6] K. Palczynski and J. Dzubiella, *J. Phys. Chem. C* **118**, 26368 (2014).
 - [7] M. Sparenberg, A. Zykov, P. Beyer, L. Pithan, C. Weber, Y. Garmshausen, F. Carlà, S. Hecht, S. Blumstengel, F. Henneberger, and S. Kowarik, *Phys. Chem. Chem. Phys.* **16**, 26084 (2014).

- [8] J. Hu, N. Aghdassi, S. Bhagat, Y. Garmshausen, R. Wang, N. Koch, S. Hecht, S. Duhm, and I. Salzmann, *Adv. Mater. Interfaces* **7**, 1901707 (2019).
- [9] L. Athouel, G. Froyer, and M. Riou, *Synth. Met.* **57**, 4734 (1993).
- [10] R. Resel, N. Koch, F. Meghdadi, G. Leising, L. Athouel, G. Froyer, and F. Hofer, *Cryst. Res. Technol.* **36**, 47 (2001).
- [11] R. Resel, *J. Phys.: Condens. Matter* **20**, 184009 (2008).
- [12] R. G. Della Valle, E. Venuti, A. Brillante, and A. Girlando, *ChemPhysChem* **10**, 1783 (2009).
- [13] M. Yoneya, M. Kawasaki, and M. Ando, *J. Mater. Chem.* **20**, 10397 (2010).
- [14] M. Yoneya, M. Kawasaki, and M. Ando, *J. Phys. Chem. C* **116**, 791 (2011).
- [15] K. Kim, E. J. G. Santos, T. H. Lee, Y. Nishi, and Z. Bao, *Small* **11**, 2037 (2015).
- [16] A. O. F. Jones, B. Chattopadhyay, Y. H. Geerts, and R. Resel, *Adv. Funct. Mater.* **26**, 2233 (2016).
- [17] T. Suzuki, K. Yagyu, and H. Tochihara, *J. Phys. Chem. C* **123**, 2996 (2019).
- [18] O. M. Roscioni, G. D'Avino, L. Muccioli, and C. Zannoni, *J. Phys. Chem. Lett.* **9**, 6900 (2018).
- [19] G. D'Avino, L. Muccioli, and C. Zannoni, *Adv. Funct. Mater.* **25**, 1985 (2015).
- [20] R. Ruiz, D. Choudhary, B. Nickel, T. Toccoli, K.-C. Chang, A. C. Mayer, P. Clancy, J. M. Blakely, R. L. Headrick, S. Iannotta, and G. G. Malliaras, *Chem. Mater.* **16**, 4497 (2004).
- [21] A. Lorenzoni, M. Muccini, and F. Mercuri, *Adv. Theory Simul.* **2**, 1900156 (2019).
- [22] A. Gerlach, S. Sellner, S. Kowarik, and F. Schreiber, *Phys. Status Solidi A* **205**, 461 (2008).
- [23] F.-J. Meyer zu Heringdorf, M. C. Reuter, and R. M. Tromp, *Nature (London)* **412**, 517 (2001).
- [24] S. Pratontep, M. Brinkmann, F. Nüesch, and L. Zuppiroli, *Phys. Rev. B* **69**, 165201 (2004).
- [25] S. Kowarik, A. Gerlach, S. Sellner, F. Schreiber, L. Cavalcanti, and O. Kononov, *Phys. Rev. Lett.* **96**, 125504 (2006).
- [26] R. Ruiz, B. Nickel, N. Koch, L. C. Feldman, R. F. Haglund, A. Kahn, and G. Scoles, *Phys. Rev. B* **67**, 125406 (2003).
- [27] N. Shioya, R. Murdey, K. Nakao, H. Yoshida, T. Koganezawa, K. Eda, T. Shimoaka, and T. Hasegawa, *Sci. Rep.* **9**, 579 (2019).
- [28] G. Duva, A. Mann, L. Pithan, P. Beyer, J. Hagenlocher, A. Gerlach, A. Hinderhofer, and F. Schreiber, *J. Phys. Chem. Lett.* **10**, 1031 (2019).
- [29] S. Nagai, Y. Inaba, T. Nishi, H. Kobayashi, and S. Tomiya, *Phys. Rev. Mater.* **5**, 013801 (2021).
- [30] M. Tejima, K. Kita, K. Kyuno, and A. Toriumi, *Appl. Phys. Lett.* **85**, 3746 (2004).
- [31] L. Muccioli, G. D'Avino, and C. Zannoni, *Adv. Mater.* **23**, 4532 (2011).
- [32] A. Pizzirusso, M. Savini, L. Muccioli, and C. Zannoni, *J. Mater. Chem.* **21**, 125 (2011).
- [33] M. J. Abraham, T. Murtola, R. Schulz, S. Páll, J. C. Smith, B. Hess, and E. Lindahl, *SoftwareX* **1–2**, 19 (2015).
- [34] W. Humphrey, A. Dalke, and K. Schulten, *J. Mol. Graph.* **14**, 33 (1996).
- [35] A. C. Wright, *J. Non-Cryst. Solids* **179**, 84 (1994), Proceedings of the First PAC RIM Meeting on Glass and Optical Materials.
- [36] M. Miletic, K. Palczynski, and J. Dzubiella, *J. Chem. Phys.* **153**, 164713 (2020).
- [37] R. G. D. Valle and H. C. Andersen, *J. Chem. Phys.* **97**, 2682 (1992).
- [38] A. A. Skelton, P. Fenter, J. D. Kubicki, D. J. Wesolowski, and P. T. Cummings, *J. Phys. Chem. C* **115**, 2076 (2011).
- [39] K. Palczynski, G. Heimel, J. Heyda, and J. Dzubiella, *Cryst. Growth Des.* **14**, 3791 (2014).
- [40] J. Wang, R. M. Wolf, J. W. Caldwell, P. A. Kollman, and D. A. Case, *J. Comput. Chem.* **25**, 1157 (2004).
- [41] M. J. Frisch, G. W. Trucks, H. B. Schlegel, G. E. Scuseria, M. A. Robb, J. R. Cheeseman, G. Scalmani, V. Barone, B. Mennucci, G. A. Petersson, H. Nakatsuji, M. Caricato, X. Li, H. P. Hratchian, A. F. Izmaylov, J. Bloino, G. Zheng, J. L. Sonnenberg, M. Hada, M. Ehara, K. Toyota, R. Fukuda, J. Hasegawa, M. Ishida, T. Nakajima, Y. Honda, O. Kitao, H. Nakai, T. Vreven, M. J. J. A., J. E. Peralta, F. Ogliaro, M. Bearpark, J. J. Heyd, E. Brothers, K. N. Kudin, V. N. Staroverov, R. Kobayashi, J. Normand, K. Raghavachari, A. Rendell, J. C. Burant, S. S. Iyengar, J. Tomasi, M. Cossi, N. Rega, J. M. Millam, M. Klene, J. E. Knox, J. B. Cross, V. Bakken, C. Adamo, J. Jaramillo, R. Gomperts, R. E. Stratmann, O. Yazyev, A. J. Austin, R. Cammi, C. Pomelli, J. W. Ochterski, R. L. Martin, K. Morokuma, V. G. Zakrzewski, G. A. Voth, P. Salvador, J. J. Dannenberg, S. Dapprich, A. D. Daniels, Å. Farkas, J. B. Foresman, J. V. Ortiz, J. Cioslowski, and D. J. Fox, *Gaussian 09 Revision D.01* (Gaussian Inc. Wallingford, CT, 2009).
- [42] B. H. Besler, K. M. Merz, and P. A. Kollman, *J. Comput. Chem.* **11**, 431 (1990).
- [43] See Supplemental Material at <http://link.aps.org/supplemental/10.1103/PhysRevMaterials.6.033403> for details on the equation of motion and the Hamiltonian, a list of all partial charges, and a discussion of the influence of interaction cutoffs, deposition rates, and polarity on the simulation results.
- [44] B. Hess, C. Kutzner, D. van der Spoel, and E. Lindahl, *J. Chem. Theory Comput.* **4**, 435 (2008).
- [45] T. Potocar, S. Lorbek, D. Nabok, Q. Shen, L. Tumbek, G. Hlawacek, P. Puschnig, C. Ambrosch-Draxl, C. Teichert, and A. Winkler, *Phys. Rev. B* **83**, 075423 (2011).
- [46] L. Athouël, G. Froyer, M. Riou, and M. Schott, *Thin Solid Films* **274**, 35 (1996).
- [47] R. Cantrell and P. Clancy, *Surf. Sci.* **602**, 3499 (2008).
- [48] J. S. Patel, A. Berteotti, S. Ronsisvalle, W. Rocchia, and A. Cavalli, *J. Chem. Inf. Model.* **54**, 470 (2014).
- [49] F. Colizzi, R. Perozzo, L. Scapozza, M. Recanatini, and A. Cavalli, *J. Am. Chem. Soc.* **132**, 7361 (2010).
- [50] G. Hlawacek, P. Puschnig, P. Frank, A. Winkler, C. Ambrosch-Draxl, and C. Teichert, *Science* **321**, 108 (2008).
- [51] L. Sun, S. Berkebile, G. Weidlinger, G. Koller, M. Hohage, F. P. Netzer, M. G. Ramsey, and P. Zeppenfeld, *Phys. Chem. Chem. Phys.* **12**, 3141 (2010).
- [52] F.-J. M. zu Heringdorf, *J. Phys.: Condens. Matter* **20**, 184007 (2008).
- [53] K. N. Baker, A. V. Fratini, T. Resch, H. C. Knachel, W. Adams, E. Soggi, and B. Farmer, *Polymer* **34**, 1571 (1993).